Scientific Visualization, 2026, volume 18, number 3, pages 52 - 62, DOI: 10.26583/sv.18.3.05

Image Processing Methods for the Problem of Plasma Control of the Bow Shock Wave

O.V. Kravchenko[1,A], T.A. Lapushkina[2,A, B], E.V. Reshetova[3,A], O.A. Azarova[4,A]

[A] Federal Research Center "Computer Science and Control" of the Russian Academy of Sciences, Moscow, Russia
[B] Ioffe Institute, Saint-Petersburg, Russia

[1] ORCID: 0000-0002-7651-3422, okravchenko@frccsc.ru
[2] ORCID: 0000-0001-9161-446X, tlapushkina@frccsc.ru
[3] ORCID: 0009-0001-1244-2792, ereshetova@frccsc.ru
[4] ORCID: 0000-0002-3896-2470, oazarova@frccsc.ru

Abstract

This paper presents an image processing procedure for experimental and numerical study of problems of plasma high-speed flow control. The experiments were conducted using a shock tube setup with an aerodynamic model placed in a high-speed flow. The impact zone was organized at the leading edge of the body by creating a local plasma gas discharge region. Flow visualization was performed using a pulsed laser schlieren system, which allows obtaining images of flow dynamics under the influence of discharge plasma. To extract quantitative data from the visualizations, an image processing pipeline was developed, including preprocessing, selection of the region of interest, and an adaptive thresholding setup for extracting information about the geometry of the plasma discharge luminosity region. This made it possible to perform numerical modeling of the two-dimensional Navier-Stokes equations for a viscous heat-conducting gas with a real source geometry. The plasma discharge was modeled as a localized energy deposition zone. For high-precision reconstruction of the flow field, a complex-conservative difference scheme of the second order on a shifted grid was used. The calculated position of the front of the bow shock wave (BSW) on the symmetry axis showed agreement with its position on the experimental schlieren image, confirming the qualitative adequacy of the numerical model. Quantitative comparison of the energy input the difference between the experimental and calculated values of the discharge power did not exceed 1%. The results showed that the presented image processing procedure opens up an approach to high accuracy prediction of the dynamics of high-speed flows.

Keywords: image processing, bow shock wave, plasma flow control, schlieren visualization, numerical simulation, energy deposition.

1. Introduction

Modern studies increasingly employ image processing methods, enabled by advances in various computer vision technologies. These techniques provide essential tools for analyzing experimental flow visualization data, including schlieren, shadowgraph, and photographic images. One of the significant problems detailed in [1] is to investigate simultaneously the evolution of discontinuous flows in a rectangular shock tube channel using high-speed imaging techniques to capture dynamic flow behavior. Complementing this experimental approach, a specialized code system for image processing was developed to address shock wave detection and tracking in high-speed experimental imagery. Further advancements include a modified background-oriented schlieren (BOS) image processing method [2], which was specifically designed to mitigate inaccuracies when analyzing millimeter-scale objects. This

method, applied to thermal airflow imaging at controlled temperatures, incorporates critical steps such as background subtraction, object reconstruction, filtering, and edge detection. The study also explores shock wave dynamics, including distortion of a wave front and instability formation. Additionally, a computational method for shock wave detection in two-dimensional viscous and inviscid flows on Cartesian grids was introduced in [3]. This approach enables precise shock identification within viscous flow fields while providing a robust representation of shock structures.

The most commonly used methods of optical flow visualization include schlieren and shadow imaging, which allow achieving observation of density gradients in transparent media with high resolution. This gives possibilities of obtaining a quantitative and qualitative representation of the flow structure [4]. Similarly, methods combining schlieren imaging with optical flow and Navier–Stokes-based reconstructions have enabled accurate temperature field recovery in high-speed jets [5]. Traditional image processing methods such as edge detection and Hough transforms have been successfully applied to identify and track coherent flow structures such as oblique and bow shocks in shadowgraph sequences [6]. These classical computer vision approaches, also based on Canny edge detection and morphological operations, provide interpretability and require minimal training data, but require extensive algorithmic tuning and post-processing to extract physical parameters. More recent advances use machine learning and deep neural networks to automate object detection and classification in complex flow fields. Convolutional neural networks (CNNs), especially modern architectures such as YOLOv8 and VGG16, have demonstrated high accuracy in detecting shockwaves, plumes, and particle structures in shadowgraph images [7], enabling scaling and real-time analysis of large experimental datasets.

Further progress has been made through physics-informed and hybrid approaches that integrate domain knowledge into data-driven models. For instance, physics-oriented constraints derived from fluid continuity and optical equations have been incorporated into optical flow frameworks to improve motion estimation in turbulent flows visualized by shadowgraphy [8], while physics-informed neural networks (PINNs) have shown promise in reconstructing hypersonic inlet flows from limited data [9]. These approaches bridge the gap between pure data-driven models and first-principles physics, enhancing both accuracy and generalizability. Despite these advances, challenges remain in handling low-contrast features, weak reflected waves, and highly dynamic flow structures—particularly in shock tube experiments where disturbance shadows exhibit high gradient continuity and low image quality [10]. Innovative cascaded feature extraction pipelines and line-scanning techniques have begun to address these issues, demonstrating sub-5% error in velocity estimation and robustness in low-resolution conditions [11].

In the present paper we proposed the image processing techniques for extracting information of the shape of the discharge plasma area from the experimental schlieren images. The study of a flow dynamics under the influence of a discharge was supported by both experimental and numerical data. The discharge effect on the flow characteristics is clearly manifested in the high-speed flow, where it was shown that changes in the adiabatic index of the discharge-generated plasma, due to the degree of ionization and the degree of nonequilibrium, along with the thermal effects, directly affect the standoff of the bow shock wave (BSW) and aerodynamic characteristics such as the drag force [12]. The extraction of the data of source geometry from experimental images and their embedding into numerical simulations was done with the use of a partially automated image processing method that extracts the real geometry about the plasma glow region boundary and incorporates it into the Navier–Stokes solver for a more accurate reconstruction of the flow field [13]. This approach allows realistic modeling of plasma flow control, increasing the accuracy of the modeling and providing better correlation with experimental observations. Compared to detectors based on, for example, convolutional neural networks such as YOLOv8 or VGG16, the proposed threshold-based method is simple and deterministic and focuses not on data, but on physical principles in the first place. It does not require labeled training data, retains the direct interpretability of the

extracted geometry of the plasma boundary, and remains applicable to limited sets of experimental images. Neural network-based approaches assume large labeled sets of experimental images to automatically solve the problem on new images, while the proposed approach is designed to transfer physically significant source geometry directly to a numerical solver with a significantly limited amount of data, therefore, a direct correct comparison of the two approaches in this problem seems difficult.

2. Experimental setup and diagnostics

2.1 Shock tube

The experiments were conducted using an experimental setup based on a shock tube. Fig. 1 shows the schematic of the gas-dynamic circuit. Here, 1 is the high-pressure chamber, 2 is the low-pressure chamber, 3 is the measuring block, 4 is the supersonic nozzle, 5 are the optical windows, 6 is power supply to the electrodes, 7 is the working chamber, 8 is the aerodynamic model with electrodes, 9 is the damping tank, 10 is the nozzle inlet slit, 11 is the inlet cross-section, 12 is the diaphragm unit, and 13 is the exhaust channel. The working chamber 7 is attached to the end of the low-pressure chamber 2 and consists of a flat, symmetric supersonic nozzle 4 with a wall inclination angle of 11° relative to the axis. On the nozzle axis, at a distance of 23 cm from the inlet, a model (8) is placed, shaped as a semi-cylinder with a rounded front part of 1.5 cm radius and a length of 3.8 cm. A gas compressed in the shock tube, with stagnation parameters, enters the nozzle, generating a supersonic flow in the region around the model.

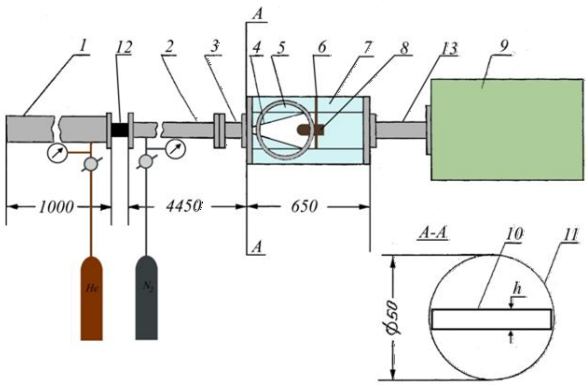


Fig. 1. Experimental setup scheme.

2.2 Schlieren visualization

Flow visualization was performed using a schlieren system (Fig. 2) illuminated by a semiconductor laser with electron-beam pumping, producing light pulses with a duration of 30 ns. The laser beam illuminates an entrance slit positioned at the focal distance from the input lens. The parallel beam passes through the region around the model via optical windows. After traversing the flow field, the beam is focused by an output lens onto the plane of a knife edge, subsequently illuminating the sensor of a Canon EOS 300D digital camera. The camera lens is adjusted to provide a sharp image of the model while fully capturing the laser illumination without clipping. The knife edge blocks half of the focused slit image, creating a dimmed background around the model on the camera sensor. During supersonic flow, density gradients associated with shock waves and other flow discontinuities refract the laser light, altering its propagation path. This refracted light is either blocked by or passes above the knife edge, resulting in regions of reduced or enhanced brightness compared to the background.

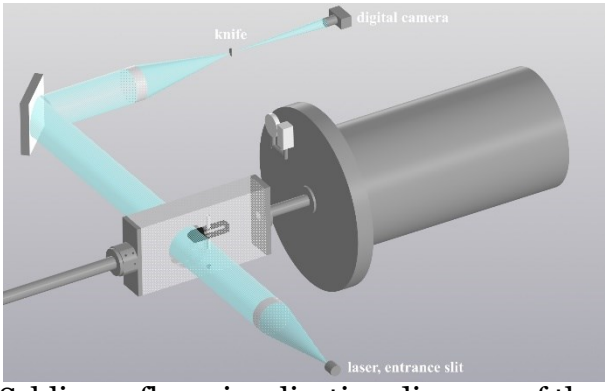


Fig. 2. Schlieren flow visualization diagram of the model.

As a result, the BSW formed during supersonic flow over the model is clearly visualized as distinct bright or dark features in the captured images.

2.3 Energy impact investigation

To influence the position of the bow shock wave, a gas discharge was organized at the leading edge of the body, creating a plasma zone near the body. The main obstacle to obtaining high-quality schlieren images was the intense self-emission of the plasma. To reduce this effect, an optical filter was used, transmitting light within the wavelength band of the laser emission at 656 nm, and a narrow collimator was placed in front of the knife edge. On the other hand, the plasma's own glow made it possible to refine the shape of the impact area during further image processing. From the flow images obtained in different experiments, the distance *d* along the nozzle axis from the model's nose to the detached shock wave was determined, and the variation of the BSW position was analyzed depending on the controlled flow conditions.

A photograph of the working chamber with the supersonic nozzle and the installed model inside is shown in Fig. 3.

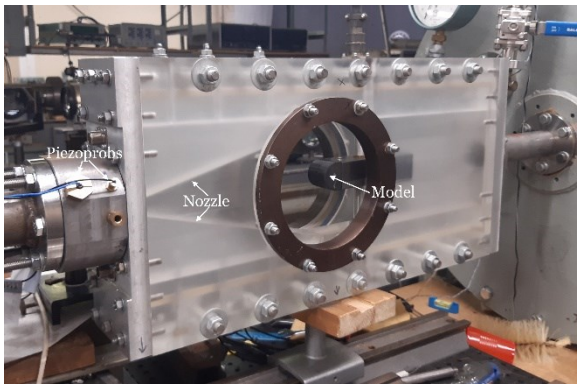


Fig. 3. Photo of the working camera.

3. Results and discussion

3.1 Schlieren-like image processing

The image processing algorithm starts with an input image (Fig. 4, left), which is preprocessed using Gaussian filtering to reduce high-frequency noise and smooth the image while preserving important flow features such as shock fronts. Afterwards, the image is normalized to enhance contrast and ensure a uniform intensity distribution across the entire data. The filtered image is then converted to grayscale to simplify further processing, since intensity variations in the luminance channel contain the main information about the flux den-

sity gradients. Next, auxiliary constructions are performed based on the assumption of axial symmetry of the problem (Fig. 4, center).

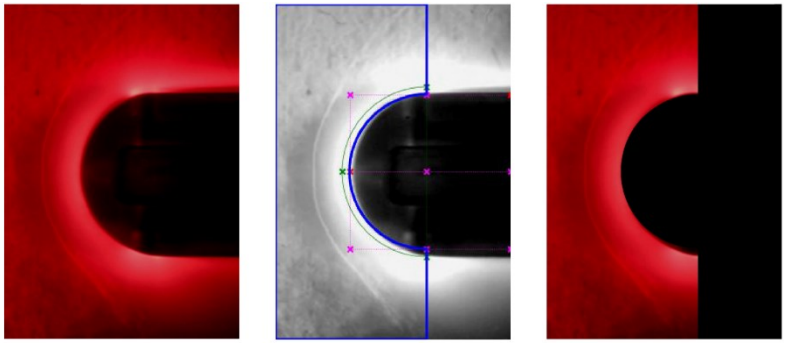


Fig. 4. Experimental image pre-processing

Finally, a region of interest (ROI) is extracted from the processed grayscale image, containing information about the area around the aerodynamic model and the inferred location of shock wave structures, which reduces the computational load and minimizes interference from irrelevant background areas (Fig. 4, right).

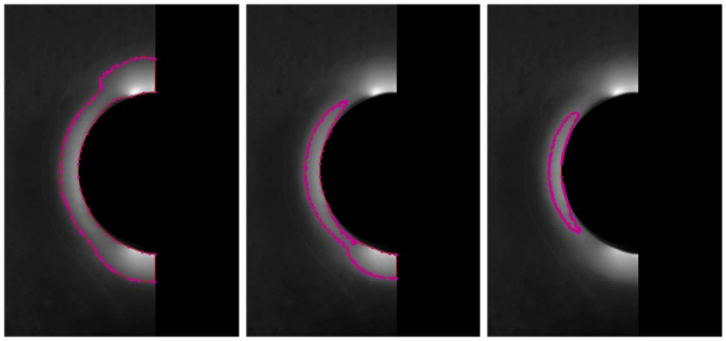


Fig. 5. Extracting the source region boundary (red line) based on the threshold value

The resulting contours describing the boundary of the plasma source region are sensitive to the choice of threshold, as shown in Fig. 5, which shows the effects of using thresholds of 80% (Fig. 5, left), 85% (Fig. 5, center), and 90% (Fig. 5, right), respectively. These thresholds are defined with respect to the intensity distribution in the grayscale image. For example, a threshold set at 85% corresponds to the intensity value above which the brightest 15% of the pixels are located. This adaptive thresholding approach provides robust boundary detection by focusing on the most significant density gradients in the flow, such as shock fronts, while filtering out low-contrast noise or background variations. The optimal threshold is selected based on visual inspection and compliance with the expected physical structures, providing an accurate representation of the flow features under different experimental conditions. The thresholds of 80%, 85% and 90% in Fig. 5 are included as an illustration of the variability of the approach for the reconstructed boundary of the plasma region. For the considered experimental frame used for contour plotting, the values of the source area ranged from approximately 0.118 at 82% to 0.096 at 85% in dimensionless units. At 86%, the area drops to 0.042, which indicates fragmentation of the selected luminosity region. The Otsu threshold value, excluding the low-intensity background, shifted to intensity levels 122-131, which corresponds to approximately the 82-85% percentile of the central area of interest. Thus, the threshold close to 85% was maintained as a physically reasonable compromise between suppressing weak background luminosity and maintaining the expected shape of the plasma source.

3.2 Numerical simulation

A numerical simulation of high-speed flow around an aerodynamic body under the influence of a discharge plasma region was carried out by solving two-dimensional Navier–Stokes equations for a viscous heat-conducting gas (xenon). The main goal of the modeling was to study the influence of localized energy deposition on the position of the BSW formed in front of the model. The schematic of the statement of problem for the numerical simulations is presented in Fig. 6.

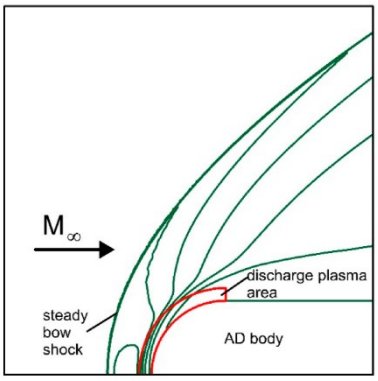


Fig. 6. Sketch of the computational domain

The plasma region created by the discharge was modeled as a steady zone of the increased characterized by the specific discharge power q (power per unit of mass), and changed thermodynamic properties, in particular, the variable adiabatic index (γ), which depends on degree of ionization and degree on nonequilibrium. The approach takes into account increased ionization and temperature in the flow due to both shock compression and the action of the discharge, where the latter is introduced as a term of the volumetric energy source in the energy equation (see details of the statement of numerical problem in [12]). Comparative analysis of the numerical results with experimental schlieren images [12] for moderate discharge parameters (I≤915 A, q<214) revealed good agreement between the position and shape of the BSW on the symmetry axis, which confirmed the reliability of the numerical model in predicting the main characteristics of a high-speed flow.

In the present study, the extracted boundaries of the discharge created plasma zone were introduced into the numerical algorithm which provided a more accurate simulation of the impact of the plasma region and made it possible to simulate high-energy discharges (I~1200A, q=550).

The computational domain (Fig. 6), defined by the parameters $0 < x < 2.5$ and $0 < y < 2.0$, was discretized on a structured grid with a node size of 2500 × 2000, which provides sufficient resolution of the flow gradient structure. The governing equations were solved in conservative divergence form [12] using a special computational code based on complex conservative difference schemes of second order accuracy in both space and time [14]. The numerical scheme uses a five-point Lax-type stencil on a shifted uniform grid, where both the primary conservative variables (density, momentum, energy) and their first spatial derivatives with respect to x and y are treated as independent unknowns and reconstructed simultaneously. It was implemented in the FlowView code package [15]. The curved boundary of the aerodynamic body is embedded into a rectangular computational grid using specially constructed approximations that use fractional cells (1/4, 1/2, 3/4) adjacent to the full cells, ensuring strict conservation of mass, momentums and energy in the entire computational domain, including the near-wall regions. The grid convergence tests are described in [12]. The determining parameters of the oncoming flow and normalizing coefficients are presented in Table 1.

Table 1. Determining parameters of the oncoming flow and normalizing coefficients

Parameter	Dimensional value	Non-dimensional value	Normalizing value
Freestream Mach number M_∞		6.8	
Adiabatic index in on-coming flow γ_∞		1.217	
Reynolds number Re		4558.9	
Prandtl number Pr		0.623	
Freestream gas density ρ_∞	0.040793 kg/m^3	1.0	$\rho_n=\rho_\infty$
Freestream gas pressure p_∞	3.1×10^3 Pa	1.0	$p_n=p_\infty$
Freestream gas temperature T_∞	1200 K (926.85 °C)	1.0	$T_n=T_\infty$
Body's diameter D	3×10^{-2} m	1.0	$l_n=D$
Freestream gas velocity u_∞	2067.96 m/s	7.502	$u_n=(p_n/\rho_n)^{1/2}=275.668$ m/s
Time t		1.0	$t_n=l_n/u_n=108.827$ μs
Specific power in the plasma region q	384.06×10^6 kW/kg	550	$q_n=p_n/(\rho_n t_n)=0.698299\times10^6$ kW/kg
Adiabatic index in the plasma region γ_s		1.31	

The fields of density, pressure, temperature, and local Mach number are shown in Fig. 7 for the steady flow mode at t=2.0, γ_s =1.258 [12] and q = 0 (without the discharge). It is evident that the initial ionization in front of the body influences the flow density and temperature to a greater extent than other parameters. Besides, one can see that the subsonic zones of high temperature are formed near the horizontal boundaries of the body. The value Re=4558.9 in Table 1 for xenon sets the scale of the viscous terms in the dimensionless Navier-Stokes system with the adopted normalization of variables which is consistent with the experimental parameters (See Table 1). The experiment is carried out in an expanding nozzle at corresponding relatively low pressure and density of the incident flow, so we used the experimental parameters of flow at the location where the model is placed in the nozzle.

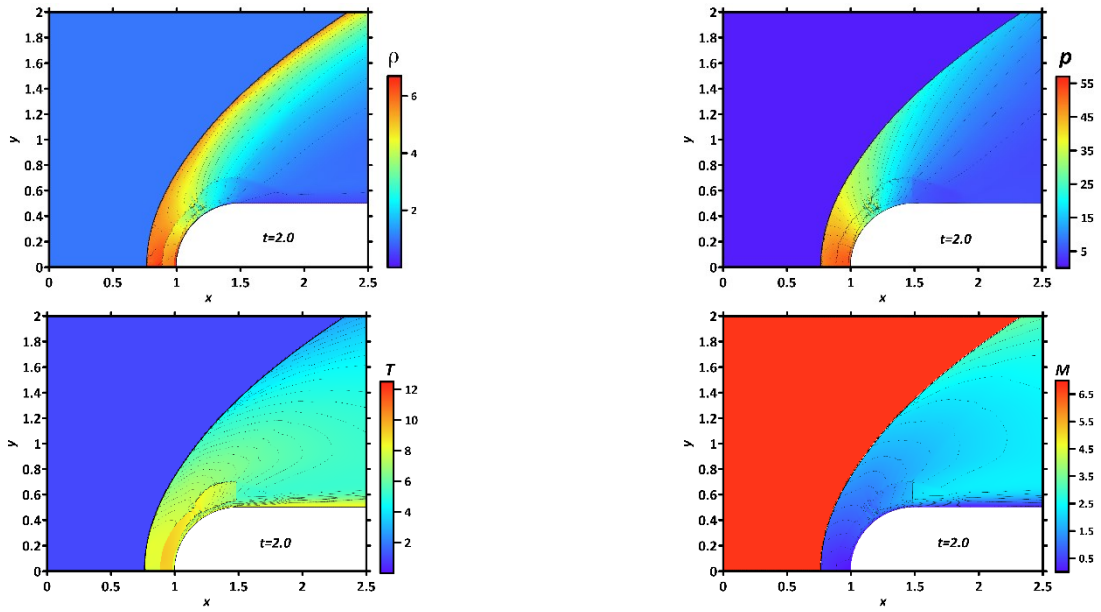


Fig. 7. Fields of density, pressure, temperature and local Mach number for q=0, steady flow

The calculated fields of density, pressure, temperature, and local Mach number for a steady supersonic flow at the specific discharge power of q = 550 are presented in Fig. 8. Fig. 8 illustrates the steady-state distributions of key flow parameters, including density (a), pressure (b), temperature (c), and local Mach number (d), evaluated at the specific discharge power of q=550. As expected, the BSW generates a pronounced region of compressed gas behind its front, characterized by significantly increased pressure and temperature values, consistent with classic hypersonic flow behavior in the absence of energy addition. However, the introduction of energy deposition alters this structure markedly. Adjacent to the body's frontal surface, a well-defined zone of rarefied gas forms, exhibiting reduced density but notably higher temperatures compared to the surrounding flow. This thermal layer arises due to the energy input's influence on local gas dynamics, effectively modifying the BSW standoff distance and creating a distinct thermophysical boundary near the body.

The determining parameters of the flow include the discharge current I=1196 A, the experimental power P_{exp}=150.70 kW, the dimensionless specific power in the plasma region q=550, and the specific heat ratio of the plasma region γ_s=1.31 [12].

The results of the calculations examining the effect of the area of the discharge energy on steady BSW position at t=2.0 are shown in Fig. 9. This analysis considers a modified adiabatic index (γ_s =1.31) within the discharge plasma region. The steady-state density fields show a correlation that increasing the specific power q, produces an increase in the standoff distance of the BSW. The mechanism of such a phenomenon was described in [16] for an air flow. This relationship is a consequence of the BSW forming within a region preheated by the discharge. Due to the significantly faster timescale of plasma formation compared to gas-dynamic evolution, the initial discharge parameters critically determine the BSW formation in the unsteady phase and, consequently, its final steady-state properties.

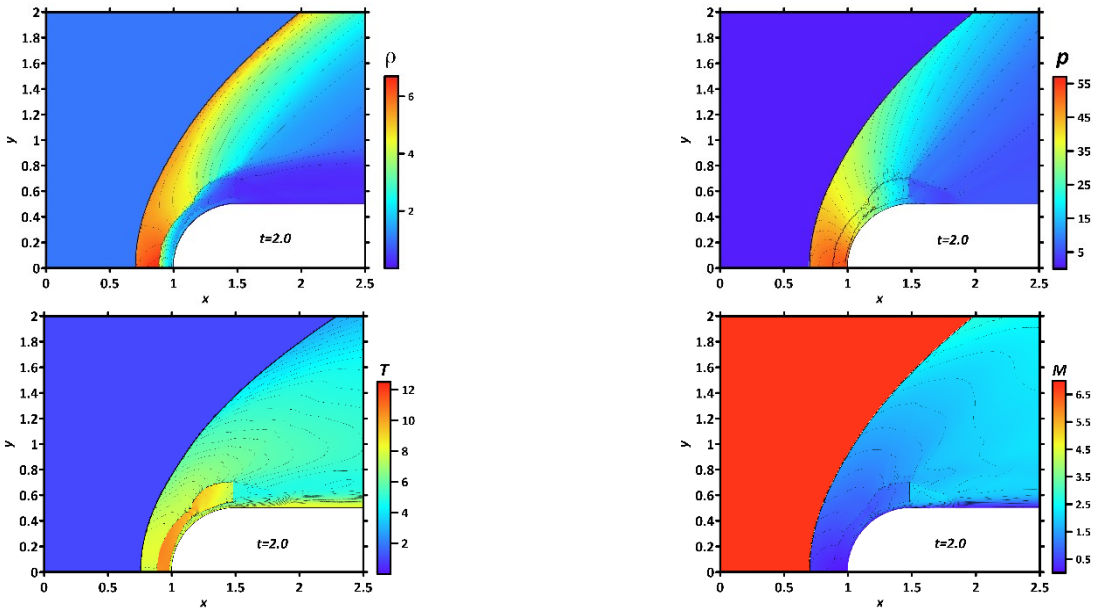


Fig. 8. Fields of density, pressure, temperature and local Mach number for q=550, steady flow

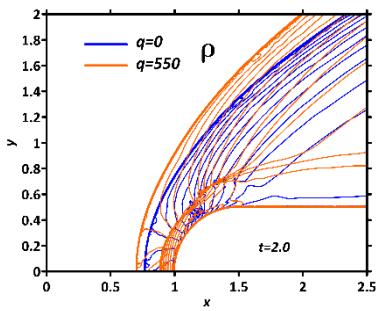


Fig. 9. Isochores of density field for q=0 and q=550

The isochores of the calculated numerical solution for the steady-state flow regime are superimposed on the experimental schlieren image for direct comparison (Fig. 10). It can be stated the sufficient agreement between the experimental image and the numerical result on the location of the BSW front on the axis of symmetry, and, in addition, the calculated discharge power was P_{calc}=152.18, which differs from the experimental value P_{exp}=150.70 kW by less than 1%.

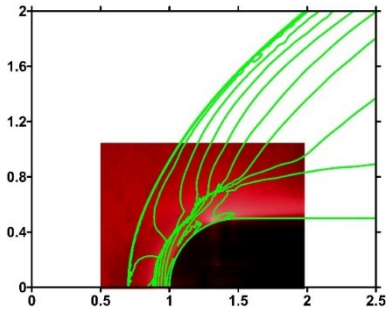


Fig. 10. Comparison of numerical flow pattern with schlieren image under the influence of a near-surface discharge in xenon, I=1196 A, P_{exp}=150.70 kW

4. Conclusion

The effect of localized energy deposition on the parameters of a high-speed flow was analyzed using a combined approach, including an experimental and numerical study based on the conducted image processing algorithm for extracting the geometry of the discharge energy deposition region. The process is simulated by solving two-dimensional Navier-Stokes equations with an energy deposition source, demonstrating an increase in bow shock wave standoff distance consistent with the experimental data. The adequacy of the model is confirmed by the good agreement between the calculated and experimental values of the discharge power and the location of the steady bow shock wave. It is shown that the presented image processing method for the schlieren flow pictures allows to increase the accuracy of the predictable flow simulation giving information on the flow characteristics, such as the position of the bow shock wave, density, pressure, temperature and local Mach number fields, etc. This provides the basis for the development of modern active control systems for high-speed flows.

Acknowledgments

The research was carried out using the infrastructure of the Shared Research Facilities «High Performance Computing and Big Data» (CKP «Informatics») of FRC CSC RAS (Moscow).

References

1. Li G., Agir M.B., Kontis K., Ukai T., Rengarajan S. Image processing techniques for shock wave detection and tracking in high speed schlieren and shadowgraph systems // J. Phys.: Conf. Ser. 2019. Vol. 1215. P. 1–9. DOI: 10.1088/1742-6596/1215/1/012021.

2. Barinov Yu.A. A new method of processing background oriented schlieren images // Tech. Phys. Lett. 2019. Vol. 45, No. 6. P. 632–634. DOI: 10.1134/S106378501906021X.

3. Fujimoto T.R., Kawasaki T., Kitamura K. Canny-Edge-Detection/Rankine-Hugoniot-conditions unified shock sensor for inviscid and viscous flows // J. Comput. Phys. 2019. Vol. 396. P. 264–279. DOI: 10.1016/j.jcp.2019.06.071.

4. Znamenskaya I.A. Methods for panoramic visualization and digital analysis of thermophysical flow fields. A review // Sci. Vis. 2021. Vol. 13, No. 3. P. 126–158. DOI: 10.26583/sv.13.3.13

5. Wu J., Zhang Z., Zhu Y., Tang Y., Guo R., Chen J., Xing Z. An accurate temperature field reconstruction method using schlieren imaging and optical flow for high-speed flow fields // Phys. Fluids. 2025. Vol. 37, No. 1. Art. 016105. DOI: 10.1063/5.0248350

6. Doroshchenko I.A. Analysis of the experimental flow shadowgraph images by computer vision methods // Numerical Methods and Programming. 2023. Vol. 24, No. 2. P. 231–242. DOI: 10.26089/NumMet.v24r217

7. Doroshchenko I.A., Znamenskaya I.A., Sysoev N.N., Lutsky A.E. High-speed flow structures detection and tracking in multiple shadow images with matching to CFD using convolutional neural networks // Sci. Vis. 2022. Vol. 14, No. 4. P. 1-11. DOI: 10.26583/sv.14.4.01

8. Mei X., Wang Q. A physics-oriented shadowgraph motion estimation algorithm for turbulent flow structures // Aerosp. Sci. Technol. 2024. Vol. 145. P. 1-10. DOI: 10.1016/j.ast.2024.108888

9. Guo M., Deng X., Ma Y., Tian Y., Le J., Zhang H. Hypersonic inlet flow field reconstruction dominated by shock wave and boundary layer based on small sample physics-informed neural networks // Aerosp. Sci. Technol. 2024. Vol. 150. P. 1-14. DOI: 10.1016/j.ast.2024.109205

10. Du H., Yang J., Yang M., Niu T. Image processing based disturbance shock wave in shock tube characteristic extraction method // J. Mod. Opt. 2025. P. 1–11. DOI: 10.1080/09500340.2025.2493200

11. Hanfy A.H., Flaszynski P., Kaczynski P., Doerffer P. Advancements in shock-wave analysis and tracking from schlieren imaging. 2024. DOI: 10.2139/ssrn.4797840 (preprint)

12. Azarova O.A., Lapushkina T.A., Kravchenko O.V. Impact of a near-surface plasma region on the bow shock wave and aerodynamic characteristics of a high-speed model in xenon // Fluids. 2024. Vol. 9, No. 12. P. 277. DOI: 10.3390/fluids9120277

13. Kravchenko O.V., Azarova O.A., Lapushkina T.A. Image-based processing simulation of shock wave propagation through the area of ionization instability // Journal of Physics: Conference Series. 2021. Vol. 2127, No. 1. Art. 012013. DOI: 10.1088/1742-6596/2127/1/012013

14. Azarova O.A. Complex conservative difference schemes for computing supersonic flows past simple aerodynamic forms // Comput. Math. Math. Phys. 2015. Vol. 55. P. 2025–2049. DOI: 10.1134/S0965542515120039

15. Azarova O.A. FlowView software package // Russian Patent Certificate No. 2022667647, 22.09.2022, 2022. URL: https://elibrary.ru/tnixmw

16. Azarova O.A., Lapushkina T.A., Shustrov Y.A. Near-surface gas discharge effect on a steady bow shock wave position in a supersonic flow past a cylindrically blunted body in the air // Phys. Fluids 2022. Vol. 34. P. 066117.